Crystal Structure and Properties of Ru-Stoichiometric $LaSrMnRuO_6$

Rey O. Bune,[†] Maxim V. Lobanov,[†] Guerman Popov,[†] Martha Greenblatt,*[,†] Cristian E. Botez,[‡,||] Peter W. Stephens,[†] Mark Croft,[⊥] Joke Hadermann,[§] and Gustaaf Van Tendeloo[§]

Department of Chemistry and Chemical Biology, Rutgers, The State University of New Jersey, Piscataway, New Jersey 08854, Department of Physics and Astronomy, State University of New York, Stony Brook, New York 11794, Department of Physics and Astronomy, Rutgers, The State University of New Jersey, 136 Frelinghuysen Road, Piscataway, New Jersey 08854, and EMAT, University of Antwerp, Groenenborgerlaan 171, B-2020 Antwerp, Belgium

Received October 27, 2005. Revised Manuscript Received February 2, 2006

A stoichiometric $LaSrMnRuO_6$ perovskite was synthesized by a modified sol−gel method. Special precautions were taken to minimize loss of ruthenium during the synthesis. $LaSrMnRuO_6$ crystallizes with an orthorhombic perovskite structure in space group *Imma* determined by synchrotron powder X-ray diffraction; the Mn/Ru cations are disordered. A small amount of a *Pmnb* phase observed along with the major phase by electron diffraction transformed to *Imma* under the electron beam. X-ray absorption near-edge spectroscopy established the formal oxidation states as Mn^{3+} and Ru^{4+}. Magnetic studies show ferromagnetic ordering at a Curie temperature of 225 K and an anomaly at 80 K. The magnetization, at 5 K in a field of 5 T, is not completely saturated and yields 2 μ_B per formula unit, much lower than the 6 μ_B expected. Electronic-transport measurements indicate semiconductor behavior with activation energies of 19.1 meV in the 230−380 K region and 22.7 meV in the 60−180 K region. A magnetoresistance of −6% is observed near the Curie temperature in a field of 5 T.

I. Introduction

The discovery of high tunneling magnetoresistance (TMR) at room temperature in Sr_2FeMoO_6[1] stimulated a great deal of research in the field of ordered double perovskites (DPs). Perovskites with Mn and Ru as the B cations were reported previously;[2−5] three compounds shared the nominal formula $LaSrMnRuO_6$.[2,3,5] Ramesha et al.,[2] Fang et al.,[3] and Dass et al.[5] reported ferromagnetic (FM) transitions with high Curie temperatures in their $LaSrMnRuO_6$; hence, this material was a promising candidate for TMR. However, there were considerable discrepancies in the observed structural, transport, and magnetic properties of $LaSrMnRuO_6$ in the three reports. It was plausible that the conventional solid-state synthesis route used in all of the prior works led to significant ruthenium loss. This could occur because of the tendency of RuO_2 (used as the starting material for Ru) to form highly volatile RuO_4[6] at the reaction temperatures (>1000 °C). Ru deficiency could significantly alter the magnetic and transport properties of $LaSrMnRuO_6$, especially by introducing mixed-valence $Mn^{3+/4+}$ that resembles $La_{1-x}Sr_xMnO_3$ perovskites known for their high T_c values. Thus, the synthesis of stoichiometric $LaSrMnRuO_6$ was of interest.

The crystal structures of perovskites and related compounds are often distorted from ideal cubic structure ($Pm\bar{3}m$ or $Fm\bar{3}m$ in the case of B-site ordered compounds) because of octahedral tilts. Group theory provides 15 unique tilt systems out of the 23 Glazer systems for "simple" (B-site disordered) perovskites.[7] In many cases, however, the lattice metric remains strongly pseudocubic, and the reflection splittings, as well as superlattice reflections, can usually be detected only by high-resolution synchrotron X-ray or neutron diffraction or by transmission electron microscopy. The details of the actual structure (especially the B−O−B′ bond angle) govern the exchange interactions and transport properties: generally, the highest magnetic transition temperatures and lowest resistivities are obtained when the B−O−B′ angle is close to the ideal 180°.[8]

DP systems can also undergo structural transformations with decreasing temperature. In Sr_2FeMoO_6, the $Fm\bar{3}m \rightarrow I4/m$ structural transition coincides with the onset of FM

* To whom correspondence should be addressed. E-mail: martha@rutchem.rutgers.edu.
† Department of Chemistry and Chemical Biology, Rutgers, The State University of New Jersey.
‡ State University of New York, Stony Brook.
|| Current address: Department of Physics, University of Texas at El Paso, El Paso, TX 79968.
⊥ Department of Physics and Astronomy, Rutgers, The State University of New Jersey.
§ University of Antwerp.

(1) Kobayashi, K.-I.; Kimura, T.; Sawada, H.; Terakura, K.; Tokura, Y. *Nature* **1998**, *395*, 677.
(2) Ramesha, K.; Thangadurai, V.; Sutar, D.; Subramanyam, S. V.; Subbanna, G. N.; Gopalakrishnan, J. *Mater. Res. Bull.* **2000**, *35*, 559.
(3) Fang, M.; Kato, M.; Yoshimura, K.; Kosuge, K. *J. Alloys Compd.* **2001**, *317*, 136.
(4) Granado, E.; Huang, Q.; Lynn, J. W.; Gopalakrishnan, J.; Ramesha, K. *Phys Rev. B* **2004**, *70*, 214416.
(5) Dass, R. I.; Yan, J.-Q.; Goodenough, J. B. *Phys Rev. B* **2004**, *69*, 094416.
(6) Ginzburg, S. I.; Ezerskaya, N. A.; Prokof'eva, I. V.; Fedorenko, N. V.; Shlenskaya, V. I.; Bel'skii, N. K. *Analytical Chemistry of Platinum Metals*; Wiley & Sons: New York, 1975.
(7) Howard, C. J.; Stokes, H. T. *Acta Crystallogr., Sect. B* **1998**, *54*, 782.
(8) Mitchell, R. *Perovskites: Modern and Ancient*; Almaz Press Inc.: Thunder Bay, ON, 2002.

10.1021/cm052371q CCC: $33.50
Published on Web 04/13/2006

order, and the structural (tilt magnitude) and magnetic (refined moment magnitude) order parameters scale with each other.[9] In the related Ca_2FeReO_6 compound, phase separation into at least two monoclinic phases with close lattice parameters occurs.[10,11]

In the present article, we report the preparation of stoichiometric $LaSrMnRuO_6$, which is reproducible with a minimum level of Ru deficiency by a modified sol−gel method. The crystal structure was analyzed by high-resolution synchrotron powder X-ray diffraction (SPXD) and electron diffraction (ED). Temperature-dependent DC magnetization and transport-property measurements and X-ray absorption near-edge spectroscopy (XANES) data are also presented.

II. Experimental Section

To minimize Ru loss during the synthesis of $LaSrMnRuO_6$, we used a novel synthesis technique based on the citrate sol−gel route reported for the preparation of $Sr_{1-x}La_xRu_{1-x}Fe_xO_3$.[12] Stoichiometric quantities of La_2O_3 (predried at 1000 °C), $SrCO_3$, $Mn(NO_3)_2$ (48.1 wt % solution in nitric acid), and $RuNO(NO_3)_3$ were dissolved in a minimum quantity (∼40 mL) of 7% HNO_3, to which ∼10 mL of ethylene glycol and ∼10 g of citric acid were added. The solution was transferred to an evaporating dish and heated on a hot plate until the mixture formed a dried citrate.

The dried citrate was decomposed overnight in a muffle furnace at 500 °C, and the product was pressed into a pellet. The pellet was wrapped in platinum foil and placed in a platinum crucible, which was covered with another platinum crucible. These platinum crucibles were placed in a large alumina crucible and surrounded by $SrRuO_3$ powder; the whole ensemble was covered with a smaller alumina crucible. The sample was heated in air at 800 °C with intermediate grindings and pelletizing until there was no change in the powder X-ray diffraction pattern (∼150 h). The product was then heated at 1100 and 1200 °C for 24 h each and at 1260 °C for several hours.

Room-temperature synchrotron powder X-ray diffraction (SPXD) data were collected on the X3B1 beamline at the National Synchrotron Light Source (NSLS), Brookhaven National Laboratory, with the sample in a capillary of 1 mm nominal diameter. X-rays of wavelength 0.6996 Å were selected by a double Si(111) monochromator and calibrated with a NIST1976a corundum standard. The intensity of the incoming beam was monitored by an ion chamber and normalized for the decay of the primary beam. After being diffracted from the powder sample, the beam was analyzed with a Ge(111) crystal. Rietveld refinements of SPXD data were performed with the GSAS/EXPGUI suite.[13,14]

Electron diffraction (ED) was performed on a Philips CM20 microscope with a LINK-2000 EDX attachment, as well as on a JEOL 4000EX, on which the high-resolution electron microscopy (HREM) images were also taken.

The Ru $L_{2,3}$-edge and Mn K-edge X-ray absorption spectroscopy (XAS) measurements were performed on beam line X-19A at the Brookhaven National Synchrotron Light Source with a double-crystal [Si(111)] monochromator. The Ru and Mn XAS measurements were made in the electron yield and fluorescence modes, respectively. For the Mn K-edge measurements, a standard was run simultaneously for a precise energy calibration, with a relative accuracy of about 0.03 eV. Standard samples were run frequently in the Ru measurements for calibration, with a lower accuracy of about 0.1 eV. The spectral data were treated by subtracting the linear energy-dependent background before the edge, yielding a constant average absorption coefficient step (normalized to unity) 100 eV above the edge.

DC magnetic susceptibility measurements were performed with a Quantum Design SQUID magnetometer (MPMS-XL) in an applied field of 1000 Oe in both field-cooled (FC) and zero-field-cooled (ZFC) modes. Field-dependent measurements of the magnetization were performed up to a maximum field of 50 kOe. Electronic-transport measurements were made by a 4-point-probe technique in the temperature range 5−400 K.

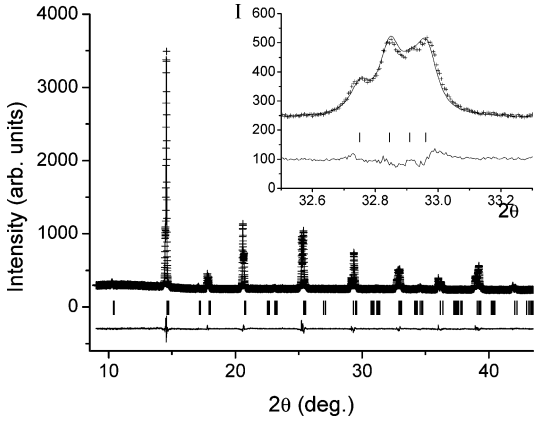

Figure 1. Synchrotron powder X-ray diffraction pattern of $LaSrMnRuO_6$. Crosses show the observed intensity; solid line is the calculated intensity; vertical lines (bottom) are the position of expected diffraction lines for the *Imma* space group; and bottom line is the difference between calculated and observed intensities. The inset shows the splitting of the peaks in the ∼32−33° 2θ range, which are indexed as (024), (233), (042), and (611) in *Imma*.

III. Results and Discussion

1. Crystal Structure. *(a) SPXD Data: Rietveld Refinement.* The SPXD pattern of $LaSrMnRuO_6$ showed splitting of the reflections (Figure 1, inset) but no violations of the I-lattice centering. Assuming that the distortion from the ideal perovskite structure occurs because of octahedral tilts (the most common mechanism), this confirms the presence of "out-of-phase" (− marks) octahedral tilts only. The reflections can be indexed in an I-centered orthorhombic lattice with unit cell parameters $b \approx c \approx a_p\sqrt{2}$; $a \approx 2a_p$ (a_p is the lattice parameter of the aristotype $Pm\bar{3}m$ perovskite), suggesting *Imma* (No. 74; $a^0b^-b^-$, no B-site ordering) as the only straightforward model of a Glazer tilt system (Figure 1 and Table 1).

With the lattice parameters assigned as in Table 1, there is an ambiguity concerning space group *Imma* vs *Imam*, i.e., whether the net rotation of the oxygen octahedra is about the *b* or *c* axis, which was impossible to resolve unambiguously with the present data including ED. We attempted to address this issue using the software program SPuDS,[15] which optimizes electrostatic energy by bond valence sum (BVS) type analysis and allows for selection of the tilt system

(9) Chmaissem, O.; Kruk, R.; Dabrowski, B.; Brown, D. E.; Xiong, X.; Kolesnik, S.; Jorgensen, J. D.; Kimball, C. W. *Phys. Rev. B* **2000**, *62*, 14197.
(10) Westerburg, W.; Lang, O.; Ritter, C.; Felser, C.; Tremel, W.; Jacob, G. *Solid State Commun.* **2002**, *122*, 201.
(11) Granado, E.; Huang, Q.; Lynn, J. W.; Gopalakrishnan, J.; Greene, R. L.; Ramesha, K. *Phys. Rev. B* **2002**, *66*, 064409.
(12) Mamchik, A.; Chen, I.-W. *Appl. Phys. Lett.* **2003**, *82*, 613.
(13) Larson, A. C.; Von Dreele, R. B. *LAUR 86-748*; Los Alamos National Laboratory: Los Alamos, NM, 1994.
(14) Toby, B. H. *J. Appl. Crystallogr.* **1999**, *32*, 281.

Table 1. Fractional Coordinates, Isotropic ADPs (B_{iso}), Site Occupancies, and Selected Interatomic Distances (Å) and Angles (deg) Refined by the Rietveld Method for the $LaSrMnRuO_6$[a]

atom	site	*x*	*y*	*z*	B_{iso} (Å^2)
Sr/La	4e	0	1/4	0.7542(5)	0.96(2)
Mn/Ru	4c	1/4	1/4	1/4	1.10(3)
O1	4e	0	1/4	0.3007(18)	1.1(2)
O2	8f	0.2189(9)	0	0	1.3(2)

Distances and Angles

Mn/Ru−O	2 × 1.9685(15)	4 × 1.9716(9)
∠(Mn/Ru−O1−Mn/Ru)	163.5(6)	
∠(Mn/Ru−O2−Mn/Ru)	165.9(4)	

[a] Space group *Imma*, $a = 7.79296(9)$ Å, $b = 5.51255(6)$ Å, $c = 5.55603(6)$ Å, $\chi^2 = 3.28$, $R_p = 1.87\%$, $R_{wp} = 2.07\%$

in perovskites on this basis. Usually, the tilt system that produces a minimum global instability index (GII) value is considered to be the actual space group. In the present case (for disordered B-site cation distribution), the minimum GII (GII = 0.15720 at $T = 298$ K) is achieved for the $R\bar{3}c$ ($a^-a^-a^-$) structure, whereas *Pnma* ($a^-b^+a^-$), which is found as a coexisting phase (see below in the ED section), yields nearly an identical value (GII = 0.15721). Prediction of a lower energy for $R\bar{3}c$ when the actual structure is *Pnma* is a common feature of SPuDS and is described in Chapter 2.7 of the SPuDS manual. This happens because the influence of O−O distances is ignored in the SPuDS calculation.

Why the majority phase has *Imma* ($a^0b^-b^-$) symmetry, for which a considerably higher GII of 0.17511 is calculated, is not clear, but it should be pointed out that BVS (in its original implementation as the calculation of formal valences from bond distances) is prone to errors in cases where Jahn−Teller cations (like Mn^{3+}) are involved. Unfortunately, at present, the Jahn−Teller M-cation option is supported for only one tilt system ($a^-b^+a^-$) in SPuDS version 2.0.

The configuration that was predicted by SPuDS for the $a^0b^-b^-$ tilt system is *Imma* with $a \approx 5.65$ Å, $b \approx 7.81$ Å, and $c \approx 5.52$ Å, or $b > c$ if transformed to a setting adopted in the ED data treatment, with *a* as the long axis (∼8 Å). However, refinement of SPXD data in this model yielded an anomalously high magnitude of the atomic displacement parameter (ADP) for the O1 site, $B_{iso} = 3.5(5)$ Å^2. In contrast, refinement with axes switched ($b < c$) did not lead to any anomaly in the ADP value $B_{iso}(O1) = 1.1(2)$ Å^2. Consequently, the latter setting ($b < c$) was chosen and used in all further refinements.

Importantly, the refinement results support the absence of a substantial Ru deficiency. There is no anomaly in the magnitude of B-site ADP; $B_{iso} = 1.10$ Å^2, and refinement of the Ru fractional occupancy did not yield significant deviations from the nominal stoichiometry. This is also consistent with the EDX analysis results (vide infra). Note that the magnitudes of ADPs cannot be determined with high accuracy with the present capillary data because of the indeterminacy of the absorption coefficient. Likewise, site occupancies are highly correlated with other parameters.

The Mn/Ru−O−Mn/Ru bond angles are ∼170° and deviate from the ideal 180° angle because of tilting of the octahedra. The Mn/Ru−O bond distances (∼1.96 Å) are very similar to the distances in other Mn/Ru−O compounds with similar oxidation states. For example, the Mn−O bond distance in $LaMnO_3$ is ∼1.94 Å[16] and that in Ru−O in $SrRuO_3$[17] and RuO_2[18] is ∼1.98 Å, consistent with the formal oxidation states of Mn^{3+} and Ru^{4+} in $LaSrMnRuO_6$ as determined by XANES (vide infra).

The close values of the effective ionic radii of Mn^{3+} (high spin (HS), 0.645 Å), and Ru^{4+} (low spin (LS), 0.620 Å)[19] and a charge difference of only one renders B-site ordering unlikely. In any case, usual checkerboard ordering would imply symmetry reduction to monoclinic, *Imma* to *I*2/*m*, and no evidence of such distortion was observed in either the SPXD or ED data (vide infra), consistent with a random distribution of Ru and Mn ions on the B-site of the perovskite.

(b) Electron Diffraction (ED) and Electron Microscopy (EM). ED and EM were undertaken to confirm the space group used to refine the SPXD data, resolve the *b* and *c* axis ambiguity discussed above, confirm that the compound is single phase, and determine the chemical composition by EDX.

Transmission electron microscopy (TEM) experiments showed the presence of two phases. Images have been obtained with a low-intensity beam in an attempt to avoid damaging the sample. When indexed using the cell parameters $b \approx c \approx a_p\sqrt{2}$; $a \approx 2a_p$, one phase shows *Pmnb* (No. 62) symmetry and the second one shows *Imma*, with observed reflection conditions as follows: *hk*0, $k = 2n$; and *h*0*l*, $h + l = 2n$ for the *Pmnb*, and *hk*0, $h = 2n$, $k = 2n$; *h*0*l*, $h + l = 2n$; and *0kl*, $k + l = 2n$ for the *Imma* phase. The presence of the 0*k*0, $k \neq 2n$, and 00*l*, $k \neq 2n$, which are forbidden reflections for the space group *Pmnb*, on the $[100]_p$ diffraction pattern is due to double diffraction.

ED patterns along the main zones of both phases are shown in Figure 2, with subscript P referring to the *Pmnb* phase and subscript I to the *Imma* phase. Measurements of the cell parameters show a slightly smaller *c* parameter than *b* parameter for the *Pmnb* phase. The differences in *d* spacing between the (200) and (011) planes are too small to make a distinction in the *Imma* phase between the $[100]_I$ and the $[011]_I$ zones, and thus this double-zone indication is shown on the ED pattern (bottom left of the diffraction pattern in Figure 2). The reflections in Figure 2 were indexed according to the $[100]_I$ zone. The same remark holds for the $[010]_I$, $[111]_I$, $[010]_P$, and $[111]_P$ zones, where the reflections are indexed as in the [010] zones (top row, middle in Figure 2). Because of this, we were unable to draw conclusions as to whether $b > c$ or $b < c$ for the *Imma* phase.

The *Pmnb* phase is unstable under the electron beam and transforms after irradiation into the *Imma* phase. The high-resolution images mainly showed the *Imma* phase (Figure 3). No amorphous domains were present in the crystals,

(15) Lufaso, M. W.; Woodward, P. M. *Acta Crystallogr., Sect. B* **2001**, *57*, 725.
(16) Huang, Q.; Santoro, A.; Lynn, J. W.; Erwin, R. W.; Borchers, J. A.; Peng, J. L.; Green, R. L. *Phys Rev. B* **1997**, *55*, 14987.
(17) Kobayashi, H.; Nagata, M.; Kanno, R.; Kawamoto, Y. *Mater. Res. Bull.* **1994**, *29*, 1271.
(18) Baur, W.; Khan, A. *Acta Crystallogr., Sect. B* **1971**, *27*, 2133.
(19) Shannon, R. D.; Prewitt, C. T. *Acta Crystallogr., Sect. B* **1969**, *25*, 925.

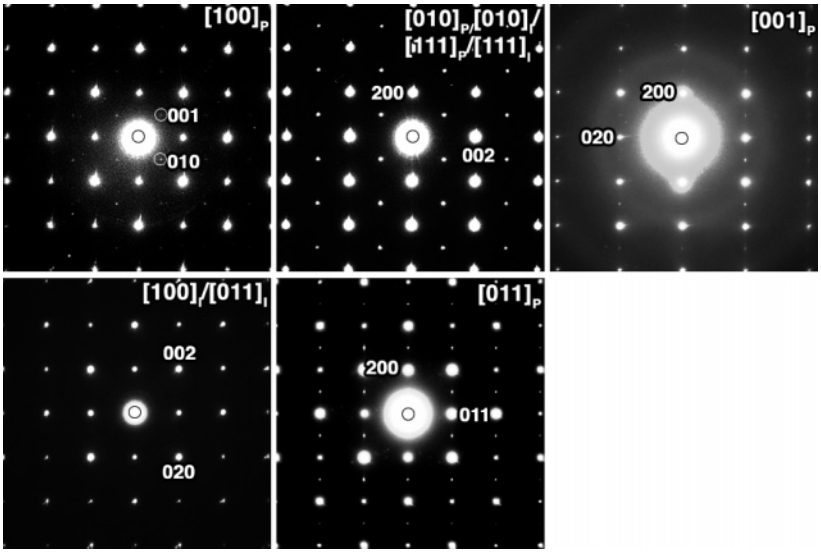

Figure 2. Electron diffraction patterns of $LaSrMnRuO_6$.

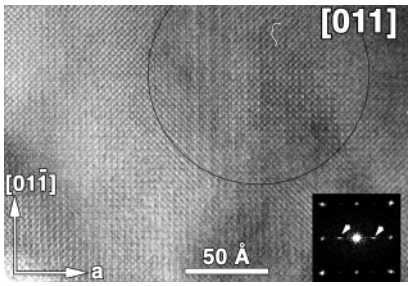

Figure 3. HREM image along [011] of the *Imma* phase, containing a small leftover of the *Pmnb* phase. The Fourier transform of the circled region is shown in the bottom right corner.

allowing us to propose that the disappearance of the *Pmnb* phase occurs through a transformation into the *Imma* phase. Using minimum exposure techniques, we were able to image the remains of the *Pmnb* phase within the *Imma* matrix. The extra reflections on the Fourier transform (indicated by arrows in the inset of Figure 3) point toward the presence of the *Pmnb* phase. The circle in Figure 3 indicates the area from which the Fourier transform was taken, which is shown in the right bottom corner of Figure 3. On the HREM images taken along the $[001]_I$ direction (not shown), domains were found within the $[001]_I$ matrix, for which the Fourier transforms corresponded to the second electron diffraction pattern (top row, middle) of Figure 2. There is no way to differentiate between these four zones, which look exactly the same in the ED pattern and are too similar to distinguish in HREM. This prevents us from extracting unambiguous information from the HREM images about either the relative size of *b* and *c* in the *Imma* phase or about the exact mechanism of transformation from *Pmnb* to *Imma*. However, a continuous phase transition is possible by symmetry between the *Imma* phase ($a^0b^-b^-$) and *Pnma* ($a^+b^-b^-$; *Pmnb* in our setting).[7] It is possible to propose that the *Pnmb*-to-*Imma* transition is just due to the removal of one tilt component.

Thus ED data (Figure 2) show a complicated two-phase picture, suggestive of a coexistence of the *Pmnb* domains in the matrix of the *Imma* phase. However, no violations of I-centering are observed in our SPXD data at room temperature, and the values of the ADPs, refined in the simple single-phase *Imma* model, are reasonable, as seen in Table 1. This indicates that the deviations from *Imma* symmetry (magnitude of the order parameter) are very small and could not be reliably refined, especially taking into account the possible coexistence of two phases. Indeed, attempted refinement in the *Pmnb* space group did not result in an improved fit. It is noteworthy that the space group symmetry reported by Refs. 4 and 5 for their $LaSrMnRuO_6$ sample is *Pbmn*, the same as the minority phase seen here in the ED of our sample; however the lattice parameters of Refs. 4 and 5 are significantly different from those of our *Imma* phase.

EDX measurements showed the cation ratio to be $La_{1.00\pm0.07}$-$Sr_{0.94\pm0.09}$ $Ru_{0.94\pm0.12}$ $Mn_{0.85\pm0.07}$, confirming the stoichiometry of the compound within experimental error.

2. XANES: Cation Oxidation State. (*a) Ru $L_{2,3}$ XANES.* The 4d transition metal $L_{2,3}$-edges are dominated by an intense white line (WL) peak (Figure 4) caused by transitions into empty 4d final states, which can be used as a probe of the 4d occupancy and 4d distribution of empty states.[20−25] The Ru L_3 (L_2)-edges in Figure 4a (4b) manifest distinct bimodal A−B feature structures with the A (B) features associated with t_{2g} (e_g) final hole states. Both the A:B intensity ratio and the center of spectral mass (chemical shift) of the WL (i.e., A + B) features are Ru valence-state indicators.

In Ru^{4+} (d^4) oxide standards RuO_2 and Sr_2RuO_4, shown in Figure 4, the A (due to 2 t_{2g} holes) feature is an unresolved shoulder on the low-energy side of the B feature (due to 4 e_g holes). Ru^{5+} (d^3) oxide standard Sr_2YRuO_6, on the other

(20) Croft, M.; Sills, D.; Greenblatt, M.; Lee, C.; Cheong, S. W.; Ramanujachary, K. V.; Tran, D. *Phys Rev. B* **1997**, *55*, 8726.
(21) Zeng, Z.; Croft, M.; Greenblatt, M. *Mater. Res. Bull.* **2001**, *36*, 705.
(22) Veith, G. M.; Greenblatt, M.; Croft, M.; Goodenough, J. B. *Mater. Res. Bull.* **2001**, *36*, 1521.
(23) Ramanujschary, K. V.; Lofland, S.; McCarroll, W. H.; Emge, T. J.; Greenblatt, M.; Croft, M. *J. Solid State Chem.* **2002**, *164*, 60.
(24) Veith, G. M.; Lobanov, M. V.; Emge, T. J.; Greenblatt, M.; Croft, M.; Stowasser, F. Hadermann, J.; Van Tendelo, G. *J. Mater. Chem.* **2004**, *14*, 1623.
(25) Huang, W.; Shuk, P.; Greenblatt, M.; Croft, M.; Liu, M. *J. Electrochem. Soc.* **2000**, *147*, 4196.

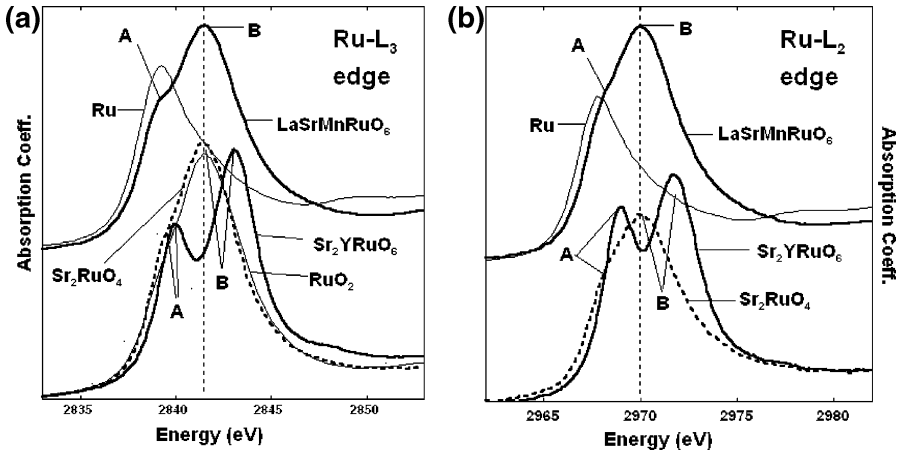

Figure 4. (a) Ru L_3-edges of $LaSrMnRuO_6$, elemental Ru, $Ru^{4+}O_2$, $Sr_2Ru^{4+}O_4$, and $Sr_2YRu^{5+}O_6$ standard. Note the A and B feature ranges associated, respectively, with the t_{2g} and e_g final states, (b) Ru L_2-edges of $LaSrMnRuO_6$, elemental Ru, $Sr_2Ru^{4+}O_4$, and $Sr_2YRu^{5+}O_6$ standard. Note the A and B feature ranges associated, respectively, with the t_{2g} and e_g final states.

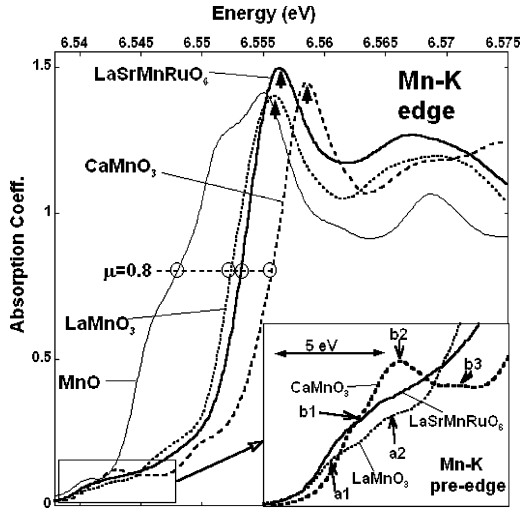

Figure 5. Mn K-edges of $LaSrMnRuO_6$ and $Mn^{2+}O$, $CaMn^{4+}O_3$, and $LaMn^{3+}O_3$ standards.

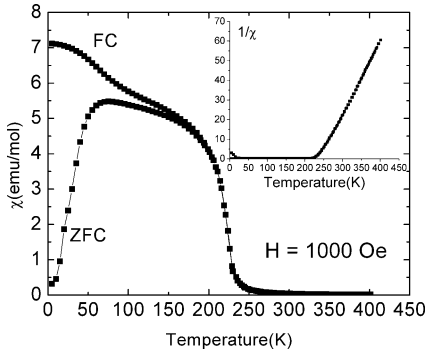

Figure 6. Temperature-dependence of the magnetic susceptibility χ of $LaSrMnRuO_6$. Inset shows $1/\chi$ vs T for $LaSrMnRuO_6$

hand, has a substantially more intense, better-resolved A feature due to the additional t_{2g} hole. In addition, the centrum of the Ru^{5+} spectrum also manifests a chemical shift to higher energy.

The shoulder A feature in the Ru $L_{2,3}$-edges of $LaSrMnRuO_6$ in Figure 4 is typical of a Ru^{4+} (d^4) material. The coincidence in energy of the B feature peaks in the Ru^{4+} standards and in $LaSrMnRuO_6$ is emphasized by a vertical dashed line in the figures. Thus, the assignment of a Ru^{4+} (d^4) configuration in $LaSrMnRuO_6$ is supported by the Ru $L_{2,3}$ XANES results.

(b) Mn K XANES. The Mn K-edge XANES measurements have proven to be useful for characterizing the Mn valence variation in manganite compounds.[20−25] In Figure 5, the Mn K-edge of $LaSrMnRuO_6$ is compared to those of the Mn^{3+}−$LaMnO_3$ and Mn^{4+}−$CaMnO_3$ perovskite standards as well as that of the Mn^{2+}−MnO compound. The most-intense peak features at these edges are related to 1s-to-4p transition splits in the detailed solid-state environment. The energy at which the absorption coefficient is roughly 80% of the total step across the edge serves as a useful measure of the chemical shift of the edge, i.e., by doing so, specific edge features, which are up- and downshifted by the environment, are averaged. The upward energy shift of the Mn K-edge, with increasing Mn valence, has been well-established in studies of the $La_{1-y}Ca_yMnO_3$ system.[20] In Figure 5, the chemical shift of the $LaSrMnRuO_6$ spectrum is close to that of $LaMnO_3$, supporting a formal trivalence assignment for the former. The modest shift of the $LaSrMnRuO_6$ edge to higher energy (relative to $LaMnO_3$) does, however, suggest a real (albeit modest) lowering of the 3d count in this compound. Here, covalency, as in all perovskite compounds, involves superposition of 3d state configurations and a nonintegral 3d occupancy.

The inset of Figure 5 shows the Mn K-preedge spectra of $LaSrMnRuO_6$, Mn^{3+}−$LaMnO_3$, and Mn^{4+}−$CaMnO_3$. The weak bimodal a1−a2 features of $LaMnO_3$ and the three (b1−b2−b3) features of $CaMnO_3$ are, respectively, typical of Mn^{3+} and Mn^{4+} perovskites. The preedge of $LaSrMnRuO_6$ appears quite similar to that of $LaMnO_3$, consistent with the main edge results above.

3. DC magnetization. DC magnetic susceptibility (χ) measurements (Figure 6) revealed a pronounced ferromagnetic (FM) transition at $T_c \approx 225$ K (determined as the maximum of the absolute value of the $\partial M/\partial T$ derivative). Curie−Weiss asymptotics yield an effective paramagnetic moment of $\mu_{eff} = 4.6\ \mu_B$ and a Weiss constant, θ, of 241 K, indicating strong FM interactions. The FM interactions are attributed to superexchange interactions between Mn^{3+} (HS, d^4) and Ru^{4+} (LS, d^4), as was previously reported in several Ru-doped manganite perovskites.[26,27] Additional indications

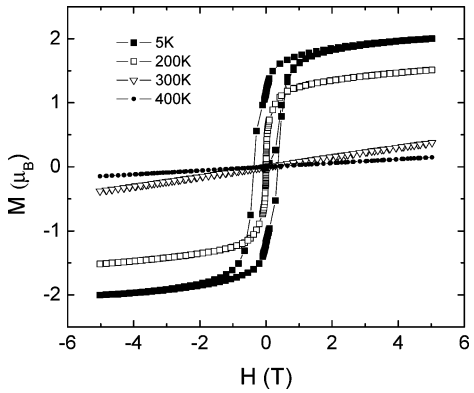

Figure 7. Field-dependent magnetization at various temperatures of $LaSrMnRuO_6$.

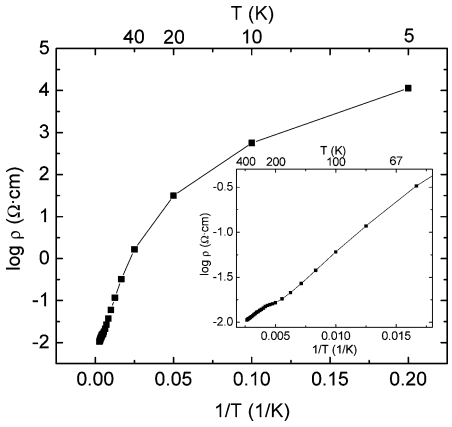

Figure 8. Log ρ vs $1/T$ plot of $LaSrMnRuO_6$.

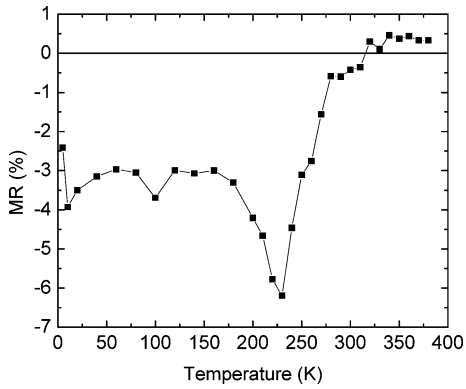

Figure 9. Magnetoresistance of $LaSrMnRuO_6$.

that the magnetic order is FM and not ferrimagnetic is evidenced by the value of θ, which is close to T_C, and the reciprocal susceptibility, which is linear with temperature in the paramagnetic region (e.g., ferrimagnetic order is typically preceded by a curved (nonlinear) $1/\chi$ vs T in the paramagnetic region). FM ordering was also seen in similar compounds reported by Granado et al.[4] and Dass et al.[5]

The calculated magnetic moment, $\mu_{calcd} = \sqrt{\sum n(n+2)}$, for the possible spin configurations of Mn^{3+} (HS, $S = 2$, $n = 4$) and Ru^{4+} (LS, $S = 1$, $n = 2$) is 5.66 μ_B, which is higher than the experimentally observed effective magnetic moment, $\mu_{eff} \approx 4.6\ \mu_B$, and is attributed to spin−orbit coupling in LS Ru^{4+}. At low T, the $\chi(T)$ curve (FC) exhibits a weak additional feature (change of slope) at ∼80 K with a large FC/ZFC hysteresis. This can be attributed to either a structural transformation or magnetic structure change. Low-temperature diffraction experiments are necessary to resolve this issue.

Measurements of magnetization (M) as a function of field (Figure 7) also support cooperative FM interactions with a coercive field of ∼0.4 T. The magnetic moment at 5 K and 5 T is 2 μ_B per formula unit, although the magnetization did not reach saturation at 5 T and 5 K. The observed μ is far less than 6 μ_B, expected for FM-ordered HS Mn^{3+} (d^4) and LS Ru^{4+} (d^4) in $LaSrMnRuO_6$. A similar observation was reported in ref 4 in which a moment of 3.66 μ_B per Mn + Ru was found by neutron diffraction. The reduced moment was proposed to originate from the strong hybridization of Ru 4d and O 2p states and frustrated exchange interactions because of random distribution of the B-site metals. Ferromagnetism, despite the reduced moment, can still occur because of strong Mn−Ru hybridization; this leads to freezing of the orientation of the Mn^{3+} e_g orbitals, broadening of the e_g valence band, and carrier-mediated FM.[4,27]

4. Electronic Transport. The temperature dependence of resistivity measured from 5 to 400 K shows semiconducting behavior with three distinct regions and a room temperature resistivity $\rho_{RT} \approx 12$ mΩ cm. Two different Arrhenius-type activation energies (E_a) can be derived from the log ρ vs $1/T$ plot (Figure 8 and inset): $E_{a1} = 19.1$ meV in the 230−380 K region, and $E_{a2} = 22.7$ meV in the 60−180 K region. The temperature of transition from E_{a1} to E_{a2} coincides with the Curie temperature (∼225 K), indicating a slight increase in band gap with the onset of magnetic order. No metal−insulator transition is observed, in contrast to $LaMnO_3$-based manganites with double-exchange interactions. The third region below 60 K does not correspond to thermally activated conduction; the transition to this behavior is observed close to the unexplained feature in magnetic susceptibility around 80 K and is possibly caused by either structural change(s) or an impurity band.

Magnetoresistance measurements showed a small negative magnetoresistance below room temperature with a peak at approximately −6%, close to T_C (Figure 9). This is consistent with a grain-tunneling type of MR, as there is no metal−insulator transition at T_C; reorientation of magnetic domains would be facilitated in an applied magnetic field near T_C.

IV. Conclusions

A new synthetic method has been successfully developed for the preparation of stoichiometric $LaSrMnRuO_6$. According to EDX and synchrotron powder X-ray data, the sample is Ru stoichiometric. The oxidation states of B-site metals were confirmed by XANES to be Mn^{3+} (d^4) and Ru^{4+} (d^4). The crystal structure was solved in the orthorhombic *Imma* space group, in contrast to previous findings of cubic symmetry ($Fm\bar{3}m$)[2,3] and *Pbnm*[5] for cation-deficient, presumably Ru-deficient analogues. Refinements of SPXD data are consistent with a disordered distribution of the Mn/Ru B-site cations. Magnetic and electronic transport measurements

(26) Raveau, B.; Maignan, A.; Martin, C.; Hervieu, M. *J. Supercond.* **2001**, *14*, 217.
(27) Martin, C.; Maignan, A.; Hervieu, M.; Autret, C.; Raveau, B.; Khomskii, D. I. *Phys. Rev. B* **2001**, *63*, 174402.

indicate that $LaSrMnRuO_6$ is a ferromagnetic semiconductor with $T_C = 225$ K; no evidence of metal−insulator transition is seen in the 5−400 K range. A small magnetoresistance of −6% is observed at ∼225 K. The properties of the Ru stoichiometric $LaSrMnRuO_6$ are significantly different from those reported previously.[2,3,5] Thus, the importance of care required to prevent the loss of Ru and thorough elemental analysis of the products is demonstrated when working with ruthenium oxide compounds at $T > 1000$ °C.

Acknowledgment. The authors are grateful to Prof. William H. McCarroll and Drs. Konstantin Lokshin, Denis Sheptyakov, El'ad Caspi, Artem Abakumov, and Viktor Poltavets for helpful discussions. This work was supported by the NSF Solid State Chemistry Grants DMR 99-07963 and DMR 02-33697. The research carried out at the NSLS at Brookhaven National Laboratory was supported by the U.S. Department of Energy, Division of Materials Sciences and Division of Chemical Sciences. The SUNY X3 beamline at NSLS was supported by the Division of Basic Energy Sciences of the U.S. Department of Energy under Grant DE-FG02-86ER45231. The work was supported in part by the program IAP V-1 of the Belgian government.

CM052371Q